Published in final edited form as:
Biochim Biophys Acta. 2015 November ; 1851(11): 1417–1427. doi:10.1016/j.bbalip.2015.08.004.

Inositol-phosphodihydroceramides in the periodontal pathogen *Tannerella forsythia*: Structural analysis and incorporation of exogenous *myo*-inositol

Zoë Anne Megson[a], **Ernst Pittenauer**[b], **Katarzyna Anna Duda**[c], **Regina Engel**[c], **Karin Ortmayr**[d,e], **Gunda Koellensperger**[e], **Lukas Mach**[f], **Günter Allmaier**[b], **Otto Holst**[c], **Paul Messner**[a], and **Christina Schäffer**[a,*]

[a]Department of NanoBiotechnology, NanoGlycobiology unit, Universität für Bodenkultur Wien, Muthgasse 11, 1190 Vienna, Austria

[b]Institute of Chemical Technologies and Analytics, Vienna, University of Technology, Getreidemarkt 9, 1060 Vienna, Austria

[c]Department of Structural Biochemistry, Priority Area Asthma & Allergy, Research Center Borstel, Leibniz-Center for Medicine and Biosciences, Parkallee 4a/4c, 23845 Borstel, Germany

[d]Department of Chemistry, Universität für Bodenkultur Wien, Muthgasse 18, 1190 Vienna, Austria

[e]Institute of Analytical Chemistry, Faculty of Chemistry, University of Vienna, Währinger Straße 38, 1090 Vienna, Austria

[f]Department of Applied Genetics and Cell Biology, Universität für Bodenkultur Wien, Muthgasse 18, 1190 Vienna, Austria

Abstract

Background—Unique phosphodihydroceramides containing phosphoethanolamine and glycerol have been previously described in *Porphyromonas gingivalis*. Importantly, they were shown to possess pro-inflammatory properties. Other common human bacteria were screened for the presence of these lipids, and they were found, amongst others, in the oral pathogen *Tannerella forsythia*. To date, no detailed study into the lipids of this organism has been performed.

Methods—Lipids were extracted, separated and purified by HPTLC, and analyzed using GC-MS, ESI–MS and NMR. Of special interest was how *T. forsythia* acquires the metabolic precursors for the lipids studied here. This was assayed by radioactive and stable isotope incorporation using carbon-14 and deuterium labeled *myo*-inositol, added to the growth medium.

*Corresponding author at: Department of NanoBiotechnology, *NanoGlycobiology* unit, Universität für Bodenkultur Wien, Muthgasse 11, 1190 Vienna, Austria. christina.schaeffer@boku.ac.at (C. Schäffer).

Conflict of interest
None of the authors have any conflict of interest.

Transparency document
The Transparency document associated with this article can be found, in the online version.

Europe PMC Funders Author Manuscripts

Results—*T. forsythia* synthesizes two phosphodihydroceramides (Tf GL1, Tf GL2) which are constituted by phospho-*myo*-inositol linked to either a 17-, 18-, or 19-carbon sphinganine, *N*-linked to either a branched 17:0(3-OH) or a linear 16:0(3-OH) fatty acid which, in Tf GL2, is, in turn, ester-substituted with a branched 15:0 fatty acid. *T. forsythia* lacks the enzymatic machinery required for *myo*-inositol synthesis but was found to internalize inositol from the medium for the synthesis of both Tf GL1 and Tf GL2.

Conclusion—The study describes two novel glycolipids in *T. forsythia* which could be essential in this organism. Their synthesis could be reliant on an external source of *myo*-inositol.

General significance—The effects of these unique lipids on the immune system and their role in bacterial virulence could be relevant in the search for new drug targets.

Keywords

Tannerella forsythia; *Myo*-inositol; Dihydroceramides; Inositol uptake; ESI–MS; NMR

1. Introduction

Tannerella forsythia is a Gram-negative anaerobic oral pathogen, a member of the so-called “red complex” of bacteria that is strongly associated with periodontitis, affecting millions of people worldwide[1-3]. The effects on the periodontium include loss of the alveolar bone around the teeth, swelling and bleeding of the gums and, in more severe cases, loss of teeth. Apart from oral health issues, emerging evidence shows a relationship between periodontal disease, cardiovascular disease and other systemic chronic diseases involving inflammation [4].

Research into bacterial phospholipid synthesis pathways has received attention related to both the study of host-pathogen interactions and the continuously growing interest in new drug targets. In particular, the study of bacterial sphingolipids has recently come into the spotlight as these compounds seem to play an important role in the host-microbe balance and could, therefore, be key to the pathogenesis of diseases [5,6]. In mammalian cells, sphingolipids have been seen to act as signaling molecules and regulators of important processes [7]. Most prokaryotic cells do not contain sphingolipids. However, they have been shown to be present in some bacteria, particularly in anaerobes, including *Sphingobacterium*, *Sphingomonas*, *Bacteroides*, and *Bdellovibrio stolpii*, some of which are pathogens or parasites able to synthesize their own membrane sphingolipids [8]. Bacterial pathogens which cannot produce sphingolipids, can utilize host sphingolipids to promote their own virulence [5]. A host sphingolipid acquired by a pathogen can be used to evade the immune system and, in turn, microbial sphingolipids incorporated into host membranes could interfere with intercellular signaling and, therefore, impair an immune response to the pathogen or cause an autoimmune response leading to the destruction of host tissues through molecular mimicry [5,9].

Recently, novel phosphorylated dihydroceramide (DHC) lipids were identified in the periodontal pathogen *Porphyromonas gingivalis* [10]. These include both low-mass and high-mass forms of phosphoglycerol DHC and phosphoethanolamine DHC lipids. The

Europe PMC Funders Author Manuscripts

phosphorylated polar head groups are linked to a core lipid structure consisting of either a 17-, 18-, or 19-carbon base in amide linkage to *iso*-17:0(3-OH) fatty acid (FA). The phosphoglycerol DHC lipids present forms with an additional *iso*-15:0 FA in ester linkage to the hydroxyl group of the *iso*-17:0(3-OH) FA. Other bacteria produce lipids that are similar to these but still markedly distinct. *Sphingobacterium* species synthesize phosphoethanolamine, phosphomannose and phospho-*myo*-inositol DHCs with the long-chain base in amide linkage to either *iso*-15:0 or *iso*-15:0(2-OH) FAs [11]. Neither phosphoglycerol DHCs nor additional ester-linked FAs were reported. In turn, phosphoglycerol ceramide has been found in *Bacteroides melaningenicus* but with different FA substitutions, containing a variety of saturated and monounsaturated FAs [12], suggesting that Nichols et al. [10] found novel lipids that are distinct from those produced by other organisms. These unusual DHCs have since also been isolated from some *Bacteroides*, *Parabacteroides* and *Prevotella* species of intestinal bacteria and from the oral pathogens *T. forsythia* and *Prevotella intermedia* [9]. In addition, they have been found to stimulate pro-inflammatory responses in gingival fibroblasts, enhance autoimmunity, promote apoptosis, and accumulate in diseased gingival tissue and other host tissues distant from the sites normally colonized by the bacteria, hence leading to the hypothesis that they might form the link between periodontal disease and systemic chronic diseases involving inflammation [9,13-15].

In this study, we report novel classes of phosphorylated DHCs which are major cellular lipid components in *T. forsythia* and have a similar lipid portion to the DHCs described by Nichols et al. [10] but contain phospho-*myo*-inositol as a polar head-group, instead of phosphoglycerol or phosphoethanolamine. We describe the chemical structure of these glycosphingolipids as elucidated by ESI–MS, GC–MS and NMR, and demonstrate how *T. forsythia* can internalize radiolabeled *myo*-inositol from the growth medium and incorporate it into its inositol-containing lipids. The potential relevance of these newly identified unique DHC sphingolipids lies in their structure and presumable function, as inositol-containing sphingolipids, rarely found in bacteria, can serve as powerful signal transduction molecules and, therefore, could have an important role in the pathogen–host interaction [6,16].

2. Materials and methods

2.1. Bacterial strains, medium and culture conditions

T. forsythia strain ATCC 43037 (American Type Culture Collection, Manassas, VA, USA) was grown anaerobically at 37 °C for 4–7 days in either 1-L or 10-mL flasks in brain heart infusion medium (BHI) supplemented with *N*-acetylmuramic acid, horse serum and gentamicin, as described previously [17].

For radioisotope labeling experiments, *T. forsythia* was grown for 4 days as described above in a 10-mL batch culture in the presence of 1 μCi of [^{14}C(U)] *myo*-inositol (Biotrend, Cologne, Germany), added to the media in 10 μL of ethanol:water (9:1).

For stable isotope labeling experiments, *T. forsythia* was grown for 4 days as described above in a 250-mL batch culture in the additional presence of 400 μM deuterium labeled

myo-inositol-1,2,3,4,5,6-D6 (EQ Laboratories GmbH, Augsburg, Germany) to give a 1:1 ratio between deuterated and endogenous inositol.

2.2. General and analytical methods

All solvents were purchased reagent-grade from Roth or Sigma-Aldrich (both Vienna, Austria), unless stated otherwise.

Lipids were analyzed by HPTLC on nano-silica gel glass plates (Sigma-Aldrich) or HPTLC-silica 60 on aluminum sheets (Merck, Darmstadt, Germany) developed in chloroform:methanol:water (65:25:4), referred to here as solvent system A.

For lipid analysis by mass spectrometry (ESI–MS), lipids were either visualized after HPTLC separation under 365-nm UV-light after staining with a primuline (Sigma-Aldrich) solution [18] and then extracted from the matrix, or purified from the silica plates as described in Section 2.4.

Other lipid visualization techniques used include the multipurpose Hanessian's stain for total lipid visualization [19] and carbohydrate staining with thymol [20].

Lipids of interest were scratched from the HPTLC plate and the scratched silica matrix was placed in a glass Pasteur pipette packed with glass-wool and the lipids were eluted with chloroform:methanol (1:1). The sample was then filtered through a 0.2-μm PTFE filter (Roth) and dried under a flow of nitrogen.

2.3. Lipid extraction

One gram of lyophilized *T. forsythia* wild-type biomass was washed extensively with ethanol and acetone prior to lipid extraction in order to remove any lipid contaminants coming from the rich growth medium [21].

Lipid extraction proceeded stepwise following the method established by Bligh and Dyer [22]. Eight mL of water were added to the biomass followed by 30 mL of chloroform:methanol (1:2) and sonicated for 15 min using a probe Branson sonifier (output 4, duty cycle 40%). Subsequently, 10 mL of chloroform were added followed by 10 mL of water, performing sonication for 5 min after each addition. Phase separation was then accelerated using centrifugation (25 min, 10,000 ×*g*) and the bottom organic phase was separated and filtered through a 0.45-μm PTFE filter followed by a 0.2-μm PTFE filter. The procedure was repeated twice on the solid interphase, and the organic phases were pooled and dried yielding 30 mg of total lipids which were redissolved in chloroform:methanol (8:2) to a concentration of 6 mg/mL.

2.4. Isolation of Tf GL1 and Tf GL2 glycolipids

The glycolipids of interest, named Tf GL1 and Tf GL2, were purified separately from several HPTLC-plates by applying the sample over the full length of the silica plate (50 μg of total lipid extract per cm of baseline). The TLC plates were developed in solvent A, air-dried, and the silica gel was scratched from the glass plate as a band from 1.5 mm below to 1.5 mm above the respective R_f value. The scratched plates were then treated with

Hanessian's stain in order to ensure that Tf GL1 and Tf GL2 had been selectively removed. The lipids were then re-eluted from the combined silica matrix, as described above, filtered and dried under a flow of nitrogen. Lipids were stored at −20 °C until further analysis.

2.5. GC–MS compositional analysis

The composition of Tf GL1 and Tf GL2 was determined after methanolysis (2 M HCl/methanol, 85 °C, 2 h) and acetylation (85 °C, 10 min) by GC–MS. FAs were additionally recovered from the chloroform phase after hydrolysis (4 M HCl, 100 °C, 4 h) and neutralization (5 M NaOH, 100 °C, 30 min) and detected by GC–MS as methyl esters (diazomethane, 10 min, 22 °C). In order to determine the position of the hydroxy groups, after evaporation to dryness, hydroxyl groups of methyl ester-FAs were incubated with BSTFA (4 h, 65 °C) and measured as TMS derivatives. The identification of the detected FAs and carbon chain branching (branched or linear) was achieved based on comparison with external standards of 15:0, 16:0(3-OH) (Larodan AB, Solna, Sweden) and 17:0(3-OH) FAs (Biotrend).

For the determination of the absolute configuration of the hydroxy FAs 16:0(3-OH), 17:0(3-OH) and the most abundant 18:0-sphinganine, Tf GL2 was treated with 48% aqueous HF (4 °C, 48 h) in order to cleave the 1-P-*myo*-inositol moiety. The remaining ceramide (200 μg) was subjected to methanolysis (2 M HCl/MeOH, 85 °C, 4 h), peracetylated and analyzed by GC–MS by use of D-*erythro*-sphinganine C18 and L-*threo*-sphinganine C18 (Sigma-Aldrich) as authentic standards. The obtained sample was further hydrolyzed (4 M HCl, 100 °C, 30 min) and the OH-FAs analyzed by GC–MS after L-phenylethylamide derivatization [23].

GC–MS measurements were performed on an Agilent Technologies 7890A gas chromatograph equipped with a dimethylpolysiloxane column (Agilent Technologies, Santa Clara, CA, USA; HP Ultra 1, 12 m × 0.2 mm × 0.33 μm film thickness) and a 5975C series MSD detector with electron impact ionization (EI) mode under autotune condition at 70 eV. The temperature program was 70 °C for 1.5 min, then 60 °C/min to 110 °C followed by 5 °C/min to 320 °C, held for 10 min.

2.6. ESI–MS analysis

Mass spectrometric measurements of purified lipid samples (see *2.4*) were performed on an Esquire 3000^{plus} 3D-quadrupole ion trap mass spectrometer (Bruker Daltonics, Bremen, Germany) in the negative-ion mode electrospray ionization (ESI–MS). Mass calibration was done with a commercial mixture of perfluorinated trialkyltriazines (ES Tuning Mix, Agilent Technologies, Santa Clara, CA, USA). All analytes were dissolved in methanol hypergrade LC–MS quality (Merck) to a concentration of ~1 mg/mL. Direct infusion experiments were carried out using a Cole Parmer model 74900 syringe pump (Cole Parmer Instruments, Vernon Hills, IL, USA) at a flow rate of 2 μL/min. Full MS-scans were acquired in the range *m*/*z* 100–1300 with the target mass set to *m*/*z* 1200. Further experimental conditions include: drying gas temperature, 200 °C; capillary voltage, −4 kV; skimmer voltage, 40 V; octapole and lens voltages, according to the target mass set. Helium was used as a buffer gas for full scans. Mass spectra were averaged during a data acquisition time of 0.5 to 1 min and one analytical scan consisted of three successive micro scans resulting in 20 and 40 analytical

scans, respectively, for the final mass spectrum. For all low-energy CID-MS^2 experiments the precursor ion mass was selected at an isolation and activation width of 4 Da. The fragmentation amplitude for dissociating the precursor ions was set to 0.45–0.5 V and the corresponding CID-spectra were collected for at least one minute.

2.7. Nuclear magnetic resonance spectroscopy of Tf GL2

Prior to NMR analyses, purified Tf GL2, 1-P-*myo*-inositol (Sigma-Aldrich), L-*threo*-sphinganine C18 (Sigma-Aldrich) and D-*erythro*-sphinganine C18 (Sigma-Aldrich) were dissolved in deuterated methanol (Deutero GmbH, Kastellaun, Germany) and placed in 5-mm NMR tubes.

All 1D (^{1}H, ^{13}C and ^{31}P) and 2D NMR ^{1}H,^{1}H COSY, TOCSY as well as ^{1}H,^{13}C HSQC, ^{1}H,^{13}C HMBC (only for Tf GL2), and ^{1}H,^{31}P HMQC experiments performed on Tf GL2 and 1-P-*myo*-inositol were recorded at 27 °C on a Bruker DRX Avance III 700 MHz spectrometer (operating frequencies of 700.75 MHz for ^{1}H NMR, 176.2 MHz for ^{13}C NMR and 283.7 MHz for ^{31}P) and standard Bruker software (TopSpin ver. 3.2). COSY and TOCSY experiments were recorded using data sets (t1 by t2) of 4096 by 512 points, with 6 scans for COSY, and 16 for TOCSY. The TOCSY experiments were carried out in the phase-sensitive mode with mixing times of 120 ms. The ^{1}H,^{13}C correlations measured in the ^{1}H-detected mode *via* HSQC-DEPT with proton decoupling in the ^{13}C domain and HMBC spectra were acquired using data sets of 4096 by 512 points and 64 scans (HSQC) and 80 scans (HMBC) for each t1 value. HMBC spectra were adjusted to *J* coupling constant value of 145 Hz and long range proton carbon coupling constant of 10 Hz. Chemical shifts were reported relative to internal methanol (δ_H 3.34, δ_C 49.86) [24] or external phosphoric acid (δ_P 0.0) [25].

2.8. Incorporation of radiolabeled myo-inositol into T. forsythia lipids

The study of radiolabeled inositol incorporation was based on procedures described previously with substantial modification[26-28]. *T. forsythia* was grown in the presence of 1 μCi of [^{14}C(U)] *myo*-inositol (specific radioactivity 200–250 mCi/mmoL) as described in Section 2.1. After 4 days of growth, the biomass was pelleted and lipids were extracted using the Bligh–Dyer method [22]. 80 μL of water were added to the wet biomass followed by 300 μL of chloroform:methanol (1:2), vortexed for 5 min and left shaking for an additional 10 min. Subsequently, 100 μL of chloroform were added followed by 100 μL of water, vortexing for 5 min and left shaking for 10 min, after each addition. After phase separation, the top aqueous phase was carefully removed. The bottom organic phase was then backwashed three times by addition of a 100 μL of water. The radioactivity in each wash fraction and in the organic phase was determined using a liquid scintillation analyzer Tri-Carb 2910 TR (Perkin Elmer, Waltham, MA, USA). The organic phase containing the extracted lipids was dried under a flow of nitrogen, redissolved in chloroform:methanol (8:2), spotted onto a HPTLC silica-gel aluminum-back plate (Merck) and then chromatographed in solvent A. The plate was then subjected to autoradiography using Kodak BioMax XAR film (Sigma-Aldrich) for three weeks at −80 °C.

2.9. Determination of free D_6-labeled and endogenous inositol in the culture medium

The determination of free deuterated and natural inositol in the medium was performed by RP–PGC–TOFMS, using known amounts of pure *myo*-inositol (Sigma-Aldrich) as standards. The medium samples were prepared by centrifugal filtration (60 min, 10 000 rpm, 4 °C; Amicon Ultra, 3 kDa MW cut-off) and diluted 1:100 in LC–MS grade H_2O (Sigma Aldrich) prior to injection. A detailed description of the chromatographic separation is provided elsewhere [29]. The chromatography column was coupled on-line to a time-of-flight mass spectrometer (Agilent 6230 LC–TOFMS) *via* a Dual AJS ESI spray chamber. ESI was performed in negative mode (45 psig nebulizer pressure, 350 °C sheath gas temperature, 11 L/min sheath gas flow, 250 °C drying gas temperature, 12 L/min drying gas flow, 110 V fragmentor voltage, 60 V skimmer voltage, 3500 V capillary voltage). MS data was acquired in the mass range 50-1000 *m/z* at an acquisition rate of 3 spectra per second. Both unlabeled and D_6-labeled *myo*-inositol were detected as formic acid adducts ($[M + COO^-]^-$, 225.0616 m/z and 231.0993 m/z, respectively) at a retention time of 3.9 min. After peak integration (Agilent MassHunter Quantitative Analysis 7.0, extraction window ±5 ppm), the peak areas were used to calculate the ratio between D_6-labeled and unlabeled inositol.

3. Results

3.1. Isolation of Tf GL1 and TF GL2

HPTLC of the Bligh–Dyer extracts from *T. forsythia* cells followed by a first screening of the primuline-stained bands using MALDI–MS (data not shown) allowed for the identification of the most abundant lipids present (phosphatidylethanolamine, monogalactosyl diacylglycerol, phosphatidic acid and cardiolipin) as well as of the phosphorylated DHC lipids previously reported by Nichols et al. [9]. In addition, we detected two novel DHC lipids which could be resolved with the solvent system A. The less abundant, more polar lipid, designated as Tf GL1, migrated with an R_f value of 0.10 and the second, more abundant lipid, designated here as Tf GL2, migrated slightly in front of Tf GL1 with an R_f value of 0.15 (Fig. 1A).

The Tf GL1 and Tf GL2 lipids were subsequently purified from several HPTLC-plates by applying the sample over the full length of the silica plate and scratching the silica from the glass plates at the corresponding R_f values. Fig. 1B shows purified Tf GL1 and Tf GL2 fractions after elution from the silica gel. Both *T. forsythia* lipids stained positive for carbohydrates as assayed with thymol. Two mg of purified Tf GL2 and 400 μg of purified Tf GL1 were recovered from the total lipid extract, representing ~20% and ~5% of the total lipid fraction, respectively.

3.2. GC–MS compositional analysis of purified Tf GL1 and Tf GL2 glycolipids

Compositional analyses of Tf GL1 and Tf GL2 revealed the presence of inositol, linear 16:0(3-OH) FA, branched 17:0(3-OH) FA as well as sphinganine with a long-chain-length of 17, 18 and 19 carbon atoms. Tf GL2 contained additionally a branched 15:0 FA. The most prominent signals belonged to 17:0(3-OH) FA and 18:0 sphinganine. GC–MS spectra of the sample after methanolysis also contained low intensity signals for glycerol, 16:0, 18:1

and 18:0 FA. However, further analyses by ESI–MS and NMR (see Sections 3.3. and 3.4. below) did not provide evidence that the aforementioned compounds were a structural part of Tf GL1 and Tf GL2. The GC–MS analyses performed on the dephosphorylated Tf GL2 revealed that the 18:0 sphinganine possessed an *erythro* configuration and both hydroxy FAs were R configured.

3.3. ESI–MS analyses of purified Tf GL1 and TF GL2 glycolipids

Negative-ion ESI–MS spectra of purified Tf GL1 and Tf GL2 (Fig. 2) revealed five $[M–H]^–$ ions for each lipid sample corresponding to the deprotonated lipid species of M_1–M_5, where M stands for the neutral mass of a given molecular species. Tf GL1 consisted mainly of the deprotonated ions of M_1, *m/z* 768; M_2, *m/z* 782; M_3, *m/z* 796; M_4, *m/z* 810; and M_5, *m/z* 824. The corresponding signals for Tf GL2 were M_1, *m/z* 992; M_2, *m/z* 1006; M_3, *m/z* 1020; M_4, *m/z* 1034; and M_5, *m/z* 1048. The spacing of 14 Da between the M_1–M_5 species is indicative of variations in FA chain length by single $[–CH_2–]$ groups, which is typical for bacteria.

Other ions present were the deprotonated sodium chloride adducts of M_3 and M_4. Both samples revealed a markedly similar quantitative distribution of M_1–M_5, with M_4 being the most predominant. The mass difference between the ions of Tf GL1 and Tf GL2 was 224 Da, which could correspond to a missing 15:0 FA in the Tf GL1 structure as compared to Tf GL2, indicating that Tf GL1 and Tf GL2 could be low- and high-mass forms of a single lipid class.

3.3.1. CID–MS^2 of Tf GL1 and Tf GL2—CID–MS^2 of Tf GL1 revealed major product ions for all four of the $[M_{2–5}–H]^–$ precursor ions (Fig. 3, Table 1). The resulting spectrum for each parent ion included peaks corresponding to the loss of inositol ± H_2O, $[M–H – (162 / 180)]^–$, loss of an amide-linked 16:0(3-OH) or 17:0(3-OH) FA, $[M–H – (254 \text{ or } 268)]^–$, and loss of the inositol and partial loss of the latter FA forming a McLafferty ion, $[M–H – (212 \text{ or } 226)]^–$ [30].

CID–MS^2 of $[M_3–H]^–$ for Tf GL1 proved the parent ion to be a mixture of two separate species of equal mass as both *m/z* 570 ($[M–H – 226]^–$) and *m/z* 584 ($[M–H – 212]^–$) McLafferty ions were present amongst the product ions indicating the presence of both amide-linked 16:0(3-OH) and amide-linked 17:0(3-OH) FAs. In addition, complete loss of this amide-linked hydroxy-FA revealed two separate ions (*m/z* 528 and 542) indicating that carbon chain length variations occurred also in the remaining core-lipid structure.

CID–MS^2 of Tf GL2 also revealed product ions for all four of the $[M_{2–5}–H]^–$ precursor ions (Fig. 4, Table 1). The detected product ions corresponded to the loss of inositol ± H_2O, $[M–H – (162 / 180)]^–$, but did not result in the previous McLafferty ions but in a loss of an ester-bonded 15:0 FA, forming a double bond in the remaining structure, $[M–H – 242]^–$, partially accompanied by the additional loss of the inositol ± H_2O, $[M–H – (404 / 422)]^–$. Loss of the ester-bonded 15:0 FA was followed by a full loss of the amide linked 16:0(3-OH) or 17:0(3-OH) FA $[M–H – (478 \text{ or } 492)]^–$, which are 3-hydroxy FAs as determined by GC–MS and the McLafferty ions formed in the CID–MS^2 of Tf GL1.

The lower molecular-mass species, Tf GL1, clearly showed two diagnostic low mass product ions for phospho-inositol at *m*/*z* 241 and 259 (which could not be found in Tf GL2 due to the low mass cut-off of the 3D-ion trap MS utilized) and presented peaks at *m*/*z* 528, 542 and 556 which also appeared as minor product ions in the higher molecular-mass species. These ions could be assigned to a sphinganine (dihydroceramide)-phospho-inositol structure where the sphinganine presents variations in the chain length assigned as 17:0 sphinganine, 18:0 sphinganine and 19:0 sphinganine, respectively.

All resulting major precursor and product ions are summarized in Table 1, along with how the variations in carbon chain lengths of both the sphinganine and the amide-linked 3-hydroxy FAs result in the lipid species M_2 to M_5. The most abundant M_4 for both Tf GL1 and Tf GL2 corresponded to the species having 18:0 sphinganine and the amide-linked 17:0(3-OH) FA, in good agreement with the GC–MS data. Fig. 5 shows the structure of Tf GL1 and Tf GL2, as elucidated from the combined GC–MS and ESI–MS data, and the described fragmentation pathways in CID–MS^2.

3.4. NMR analyses of Tf GL2

The chemical nature of the more abundant Tf GL2, composed of phospho (P)-inositol linked to *erythro*-sphinganine, further substituted by amide-linked hydroxy FAs and an ester-linked 15:0 FA, could be confirmed by NMR analyses (Fig. 6, Table 2). The P-inositol was identified as 1-P-*myo*-inositol based on the chemical shifts of the authentic standard (atoms 1–6; Fig. 6). The ^1H spectrum of Tf GL2 showed, in addition to the signals of 1-P-myo-inositol, the downfield shifted multiplet at 5.27 ppm (due to the strong deshielding effect), signals from the α-methylene groups of the amide- and ester-bound FAs (2.54, 2.35 ppm), signals resonating in the region from 1.68 to 1.61 ppm (γ-methylene group of the amide bound FA and methylene group at position 4 of the sphinganine base), and the groups of signals from 1.41 to 1.27 ppm and from 0.95 to 0.88 ppm corresponding to $-CH_2-$ and terminal methyl groups of the alkyl chains, respectively. Scalar correlation of δ_H 5.27 to δ_C 172.98 and 175.78 in the HMBC spectrum enabled assignment of the signal to the β-hydroxy group of the amide linked FA, being further *O*-acylated. The ^{31}P signal at 1.84 ppm correlated with the signals at 3.92 ppm (position 1 of inositol) and 4.26 and 3.97 ppm (position 1 of the sphinganine base) as seen in the $^1H,^{31}P$ HMQC experiment, identifying the position of the phospho-ester linkage. A HSQC-DEPT experiment (Fig. 6, Table 2) provided the direct correlation of all assigned ^1H with ^{13}C signals. Comparing ^1H spectra of the Tf GL2 with the authentic standards of the *erythro* and *threo* forms of sphinganine (that differ in the $J_{2,3}$ coupling constants, being ~ 6 Hz for *erythro* and ~2 Hz for *threo*, respectively [31]), enabled the identification of an *erythro*-sphinganine in Tf GL2. Taken together, NMR analysis of Tf GL2 confirmed the structure to be composed of 1-P-*myo*-inositol phosphoester-linked to an *erythro*-sphinganine base which is substituted *via* the amide group to an R-hydroxy FA, in turn estersubstituted by a second FA.

3.5. Uptake of the glycolipid metabolite myo-inositol from the medium

A BLASTP search against the proteome of *T. forsythia* ATCC 43037 did not identify proteins homologous to the two enzymes involved in inositol synthesis, *i.e.* inositol-3-phosphate synthase and inositolmonophosphatase. This suggests that *T. forsythia* utilizes

exogenous *myo*-inositol for the synthesis of Tf GL1 and Tf GL2. In order to prove the uptake of the glycolipid precursor *myo*-inositol from the medium, *T. forsythia* was grown in the presence of [^{14}C(U)] *myo*-inositol. Lipids were extracted using the Bligh–Dyer method and the organic phase was backwashed several times with water to insure complete removal of non-incorporated radiolabeled inositol from the organic phase. The latter fraction (containing about 0.2% of the radioactive precursor initially added) was spotted onto a HPTLC plate and separated using solvent system A. After a 3-week exposure time, two bands were clearly visible at the exact R_f values of 0.10 and 0.15 corresponding to Tf GL1 and Tf GL2, respectively (Fig. 7). This indicated that *T. forsythia* is able to import inositol from the medium and incorporate it into its lipids. No other bands were detected, indicating that [^{14}C(U)] *myo*-inositol was solely incorporated into Tf GL1 and Tf GL2.

3.6. Tf GL2 labeling with D_6-labeled myo-inositol

Quantification of free inositol in the medium revealed its presence at an approximate concentration of 400 μM, as estimated by using an external *myo*-inositol standard. D_6-labeled *myo*-inositol was then added to the medium before inoculation to give a ratio between deuterated and unlabeled inositol of close to 1:1. The ratio at the beginning of the culture and after harvesting the biomass was experimentally determined as 1.05 and 1.03, respectively. Tf GL2 was then purified and subjected to ESI–MS analysis. The ratio between deuterated and unlabeled Tf GL2 was found to be 1.11 (Fig. 8), demonstrating that the isotopic distribution of D_6-labeled inositol in Tf GL2 was practically equal to that in the medium. This provides evidence that the incorporated inositol is exclusively derived from the medium.

4. Discussion

As a close relative of *Bacteroides*, the ability of *T. forsythia* to synthesize sphingolipids, an attribute rarely found amongst bacteria, is phylogenetically well justified [6]. Although the lipidome of this bacterium is poorly characterized, some of its sphingolipids are unique phosphorylated DHCs, prevalent amongst a set of common human bacteria and biologically relevant due to their putative role in eliciting an immune response [9,10,13].

In this study, we report on two new phosphorylated DHCs (Tf GL1 and Tf GL2) which are major cellular lipid components of *T. forsythia*, structurally similar to those already described [10], but containing *myo*-inositol as a polar head-group. The structure of these unusual glycolipids was elucidated by a combination of ESI–MS, GC–MS and NMR. Tf GL1 and Tf GL2 consist of phospho-*myo*-inositol linked to a core lipid structure consisting of either a 17-, 18-, or 19-carbon sphinganine base in amide linkage to either branched 17:0(3-OH) or linear 16:0(3-OH) FA which, in the higher molecular weight structure of Tf GL2, is, in turn, substituted with an additional branched 15:0 FA in ester linkage. The lipid core described here is similar to that described by Nichols et al. [10]. These authors reported only 17:0(3-OH) FA to be present in amide linkage to sphinganine. In addition, the 17:0(3-OH) FA, 15:0 FA and 17- and 19-carbon sphinganine were determined to be *iso*-branched (the 18-carbon sphinganine was reported to be linear), as determined by comparison with the synthetic standards.

It has been postulated that there exists a relationship between periodontal disease and other systemic chronic diseases where inflammation seems to be the common link [4]. The novel DHCs published by Nichols et al. [10] were seen to be present in host tissues distant from the sites of infection and evoke an inflammatory response *in vitro* [9]. Their FA substitutions are thought responsible for this observation as the lipid portion is what differs structurally from other DHCs. The finding that these core lipid structures also exist with a rare and important polar head group like inositol, often involved in protein–lipid interactions on cell surfaces [32], further increases the interaction possibilities and widens the spectra of effects this type of lipid could have on the immune system, especially when considering that inositol-containing lipids and sphingolipids, although rare in microorganisms, seem more prevalent amongst pathogenic bacteria [5,6,33]. Confirmed functional information on inositol-containing structures is known for just a few organisms [32]. The use of *myo*-inositol for the synthesis of phosphatidylinositol (PI) and other lipids is essential in eukaryotes, including pathogenic fungi and protozoa, but is rare amongst bacteria and has been described only for a small group of actinobacteria (including mycobacteria, *Streptomyces* and corynebacteria), *Bacteroidetes* (*Sphingobacterium*) and in myxobacteria and *Treponema* [33,34]. Further occurrence of inositol in bacteria includes the use of this metabolite in *Mycobacteria* for the synthesis of mycothiol, or in other bacteria to produce di-*myo*-inositol-phosphate, or it can be used as a precursor for various aminoglycoside/aminocyclitol antibiotics [34-37]. A number of bacteria can internalize *myo*-inositol and use it as a nutrient source but cannot incorporate it into biosynthetic pathways [33,38,39].

Not only is it unique to find *T. forsythia* with inositol containing lipids but it is of particular interest how the pathogen acquires this basic molecule for the synthesis of those. For the synthesis of PI, organisms either synthesize *myo*-inositol from glucose-6-phosphate or import it from the host [33]. There is a universal mechanism for the synthesis of inositol which requires the combined action of two enzymes, inositol-3-phosphate synthase (named Ino1 in yeast) and inositolmonophosphatase, both of which are highly conserved proteins between the different domains of life [27,33]. Genes homologous to *ino1* have been found in related *Bacteroides* sp. and in the uncultured, health-associated *Tannerella* sp. BU063 [40], although the physiological significance of inositol synthesis in these bacteria is not clear [34]. In contrast, no genes predicted to be involved in inositol synthesis could be identified in the genome of *T. forsythia* [41]. By adding radiolabeled *myo*-inositol to the medium of *T. forsythia* during growth, we were able to demonstrate that the organism is able to internalize this compound and incorporate it into its lipids. Moreover, labeling experiments with deuterated inositol indicated that the source of this metabolite is solely exogenous.

In some bacteria, such as in mycobacteria, PI is further built up with other sugar residues, such as mannose, to form phosphatidyl-*myo*-inositol mannosides (PIMs) [42]. In our study, no other lipids were seen to incorporate labeled *myo*-inositol, and so further derivatization of the inositol-containing lipids to form other major lipid components is not expected to occur in *T. forsythia*.

Like other bacteria residing in human hosts, *T. forsythia* has adapted to better suit its niche and has optimized its physiology to better use the nutrients and resources available, minimizing the need of *de novo* synthesis of vital components. Furthermore, this ability in *T.*

forsythia may be a key to pathogenicity. For example, when comparing this virulent strain to the health-associated *Tannerella* sp. BU063, the latter presents two *de novo* synthesizing enzymes required to convert UDP-*N*-acetyl-D-glucosamine to UDP-*N*-acetylmuramic acid, enzymes which lack in *T. forsythia* [40]. *N*-Acetylmuramic acid can be presumably scavenged by *T. forsythia* from the host in its natural habitat but has to be added to the media for growth under laboratory conditions [43]. Similarly, *T. forsythia*, unlike the harmless *Tannerella sp*. BU063, does not have any gene homologs to *ino1*, involved in inositol synthesis, but can import inositol from the medium for synthesis of major lipid components. Human serum, contained for example in the gingival crevice, contains 61 ± 12 μM of *myo*-inositol which the pathogen could exploit for this purpose [33] and hence, taken together, we hypothesize that the uptake of inositol could be a contributing factor to virulence.

In mycobacteria, internalized inositol is first phosphorylated in order to be used as a substrate for the formation of phosphatidylinositol phosphate (PIP), formed as an intermediate during the formation of PI. This led to a newly proposed mechanism for synthesis of inositol-containing lipids in bacteria, different to that in eukaryotes [27]. Here, exogenous inositol is imported *via* an inositol or a sugar transporter and then phosphorylated to form *myo*-inositol-1-phosphate which can be coupled to CDP-diacylglycerol to form the intermediate PIP, by a CDP-alcohol phosphatidyltransferase. An added dephosphorylation step would then be needed to convert PIP to PI. As in mycobacteria[16,35], no obvious transporter genes or candidates for an inositol kinase could be identified in *T. forsythia*. Jorge et al. also described a new biosynthetic pathway restricted to bacteria which does not rely on CTP-activated glycerolipids but uses instead activated inositol in the form of CDP-inositol [44]. This pathway was elucidated for *Rhodothermus marinus* (phylum *Bacteroidetes*) and implies the inositol-3-phosphate synthase gene to be located within an operon-like structure together with a L-*myo*-inositol-1-phosphate cytidylyltransferase (IPCT) and a bacterial dialkylether glycerophosphoinositol synthase (BEPIS). This operon is found in a number of different bacterial genera and a BEPIS homologue can also be found in *T. forsythia* (Tanf_07760), but the other members of the operon are not present; especially the IPCT would be needed for synthesis of activated CDP-inositol from the imported metabolite. Therefore, in this context, the physiological importance of this putative BEPIS is currently not clear.

In order to import inositol from the medium in sufficient quantity to support the synthesis of such major lipid components, representing ~25% of its membrane lipids, we would expect a designated inositol transporter to be present. The major transporter of *myo*-inositol in *Bacillus subtilis* strains and in *Lactobacillus casei* BL23 was found to be encoded by the *iol*T gene which forms part of an operon for inositol catabolism, as inositol in these organisms can be used as a nutrient source [38,39]. As done for *Mycobacterium tuberculosis* [35], *iol*T sequences were used in a BLASTP search against the proteome of *T. forsythia* ATCC 43037. Only one significant hit could be found, Tanf_07060, classified as a major facilitator superfamily (MFS) transporter of the sugar porter (SP) family. However, this gene lies within a possible operon for the uptake and use of xylose. Therefore, the capacity of this protein to act as an inositol transporter has to be verified experimentally which is now

Europe PMC Funders Author Manuscripts

subject of further studies. Identification of the responsible gene and creation of the corresponding knock-out mutant might give insight into how essential the utilization of inositol is in this pathogen.

5. Conclusion

The study performed here on the lipids of *T. forsythia*, describes the novel structures of two classes of phospho-*myo*-inositol-DHCs. Considering that these lipids make up such a large portion of the membrane, they are possibly essential in this oral pathogen which most likely obtains all of the *myo*-inositol needed from the surrounding media. The effects of these lipids on the host immune system and its implication in the virulence of this pathogen are yet to be evaluated but could help get functional information on inositol-containing lipids and could be relevant in the search for new drug targets.

Acknowledgements

We thank Katharina Jakob and Sylvia Düpow (RCB) for excellent technical assistance, and Heiko Kässner (RCB) for NMR recordings.

This study was supported by the Austrian Science Fund FWF project P24317-B22 (to C. S.) and the Doctoral Programme Biomolecular Technology of Proteins (FWF project W1224).

Abbreviations

BSTFA	*N,O*-bis(trimethylsilyl)trifluoroacetamide
CID	collision-induced dissociation
COSY	correlation spectroscopy
DHC	dihydroceramide
ESI–MS	electrospray ionization mass spectrometry
FA	fatty acid
GC–MS	gas chromatography coupled with mass spectrometry
HMBC	heteronuclear multiple-bond correlation spectroscopy
HPTLC	high-performance thin layer chromatography
HSQC–DEPT	heteronuclear single quantum coherence–distortionless enhancement by polarization transfer
MALDI–MS	matrix-assisted laser desorption/ionization mass spectrometry
NMR	nuclear magnetic resonance spectroscopy
PDHC	phosphorylated dihydroceramide
PI	phosphatidylinositol
PIP	phosphatidylinositol phosphate
PTFE	polytetrafluoroethylene

TMS	tetramethylsilane
TOCSY	total correlation spectroscopy

References

[1]. Vos T, Flaxman AD, Naghavi M, Lozano R, Michaud C, Ezzati M, Shibuya K, Salomon JA, Abdalla S, Aboyans V. Years lived with disability (YLDs) for 1160 sequelae of 289 diseases and injuries 1990–2010: a systematic analysis for the Global Burden of Disease Study 2010. Lancet. 2013; 380:2163–2196. [PubMed: 23245607]

[2]. Haffajee A, Socransky S, Patel M, Song X. Microbial complexes in supragingival plaque. Oral Microbiol. Immunol. 2008; 23:196–205. [PubMed: 18402605]

[3]. Socransky S, Haffajee A, Cugini M, Smith C, Kent R. Microbial complexes in subgingival plaque. J. Clin. Periodontol. 1998; 25:134–144. [PubMed: 9495612]

[4]. Cullinan M, Ford P, Seymour G. Periodontal disease and systemic health: current status. Aust. Dent. J. 2009; 54:S62–S69. [PubMed: 19737269]

[5]. Heung LJ, Luberto C, Del Poeta M. Role of sphingolipids in microbial pathogenesis. Infect. Immun. 2006; 74:28–39. [PubMed: 16368954]

[6]. An D, Na C, Bielawski J, Hannun YA, Kasper DL. Membrane sphingolipids as essential molecular signals for Bacteroides survival in the intestine. Proc. Natl. Acad. Sci. U. S. A. 2011; 108:4666–4671. [PubMed: 20855611]

[7]. Ohanian J, Ohanian V. Sphingolipids in mammalian cell signalling. Cell. Mol. Life Sci. 2001; 58:2053–2068. [PubMed: 11814056]

[8]. Olsen I, Jantzen E. Sphingolipids in bacteria and fungi. Anaerobe. 2001; 7:103–112.

[9]. Nichols FC, Yao X, Bajrami B, Downes J, Finegold SM, Knee E, Gallagher JJ, Housley WJ, Clark RB. Phosphorylated dihydroceramides from common human bacteria are recovered in human tissues. PLoS One. 2011; 6:e16771. [PubMed: 21347306]

[10]. Nichols FC, Riep B, Mun J, Morton MD, Bojarski MT, Dewhirst FE, Smith MB. Structures and biological activity of phosphorylated dihydroceramides of *Porphyromonas gingivalis*. J. Lipid Res. 2004; 45:2317–2330. [PubMed: 15466368]

[11]. Naka T, Fujiwara N, Yano I, Maeda S, Doe M, Minamino M, Ikeda N, Kato Y, Watabe K, Kumazawa Y. Structural analysis of sphingophospholipids derived from *Sphingobacterium spiritivorum*, the type species of genus *Sphingobacterium*. Biochim. Biophys. Acta Mol. Cell Biol. Lipids. 2003; 1635:83–92.

[12]. White DC, Tucker AN. Ceramide phosphorylglycerol phosphate a new sphingolipid found in bacteria. Lipids. 1970; 5:56–62. [PubMed: 5418209]

[13]. Nichols FC, Housley WJ, O'Conor CA, Manning T, Wu S, Clark RB. Unique lipids from a common human bacterium represent a new class of Toll-like receptor 2 ligands capable of enhancing autoimmunity. Am. J. Pathol. 2009; 175:2430–2438. [PubMed: 19850890]

[14]. Minamino M, Sakaguchi I, Naka T, Ikeda N, Kato Y, Tomiyasu I, Yano I, Kobayashi K. Bacterial ceramides and sphingophospholipids induce apoptosis of human leukaemic cells. Microbiology. 2003; 149:2071–2081. [PubMed: 12904547]

[15]. Nichols FC, Rojanasomsith K. *Porphyromonas gingivalis* lipids and diseased dental tissues. Oral Microbiol. Immunol. 2006; 21:84–92. [PubMed: 16476017]

[16]. Movahedzadeh F, Smith DA, Norman RA, Dinadayala P, Murray-Rust J, Russell DG, Kendall SL, Rison SC, McAlister MS, Bancroft GJ. The *Mycobacterium tuberculosis ino1* gene is essential for growth and virulence. Mol. Microbiol. 2004; 51:1003–1014. [PubMed: 14763976]

[17]. Tomek MB, Neumann L, Nimeth I, Koerdt A, Andesner P, Messner P, Mach L, Potempa JS, Schäffer C. The S-layer proteins of *Tannerella forsythia* are secreted via a type IX secretion system that is decoupled from protein *O*-glycosylation. Mol. Oral Microbiol. 2014; 29:307–320. [PubMed: 24943676]

Europe PMC Funders Author Manuscripts

[18]. White T, Bursten S, Federighi D, Lewis RA, Nudelman E. High-resolution separation and quantification of neutral lipid and phospholipid species in mammalian cells and sera by multi-one-dimensional thin-layer chromatography. Anal. Biochem. 1998; 258:109–117. [PubMed: 9527856]

[19]. Meiß T, Eckelt E, Basler T, Meens J, Heinzmann J, Suwandi A, Oelemann WMR, Trenkamp S, Holst O, Weiss S, Bunk B, Spröer C, Gerlach G-F, Goethe R. The *Mycobacterium avium* ssp. *paratuberculosis* specific *mptD* gene is required for maintenance of the metabolic homeostasis necessary for full virulence in mouse infections. Front. Cell. Infect. Microbiol. 2014; 4:110. [PubMed: 25177550]

[20]. Racusen D. Glycoprotein detection in polyacrylamide gel with thymol and sulfuric acid. Anal. Biochem. 1979; 99:474–476. [PubMed: 517754]

[21]. Beczała A, Duda KA, Skurnik M, Holst O. The structure of the *O*-specific polysaccharide of the lipopolysaccharide from *Yersinia enterocolitica* serotype O: 50 strain 3229. Carbohydr. Res. 2012; 359:97–101. [PubMed: 22925771]

[22]. Bligh EG, Dyer WJ. A rapid method of total lipid extraction and purification. Can. J. Biochem. Physiol. 1959; 37:911–917. [PubMed: 13671378]

[23]. Rietschel ET. Absolute configuration of 3-hydroxy fatty acids present in lipopolysaccharides from various bacterial groups. Eur. J. Biochem. 1976; 64:423–428. [PubMed: 1278168]

[24]. Fulmer GR, Miller AJ, Sherden NH, Gottlieb HE, Nudelman A, Stoltz BM, Bercaw JE, Goldberg KI. NMR chemical shifts of trace impurities: common laboratory solvents, organics, and gases in deuterated solvents relevant to the organometallic chemist. Organometallics. 2010; 29:2176–2179.

[25]. Carballo PMS, Vilen H, Palva A, Holst O. Structural characterization of teichoic acids from *Lactobacillus brevis*. Carbohydr. Res. 2010; 345:538–542. [PubMed: 20034620]

[26]. Mikusová K, Mikus M, Besra GS, Hancock I, Brennan PJ. Biosynthesis of the linkage region of the mycobacterial cell wall. J. Biol. Chem. 1996; 271:7820–7828. [PubMed: 8631826]

[27]. Morii H, Ogawa M, Fukuda K, Taniguchi H, Koga Y. A revised biosynthetic pathway for phosphatidylinositol in *Mycobacteria*. J. Biochem. 2010; 148:593–602. [PubMed: 20798167]

[28]. Morii H, Ogawa M, Fukuda K, Taniguchi H. Ubiquitous distribution of phosphatidylinositol phosphate synthase and archaetidylinositol phosphate synthase in Bacteria and Archaea, which contain inositol phospholipid. Biochem. Biophys. Res. Commun. 2014; 443:86–90. [PubMed: 24269814]

[29]. Ortmayr K, Hann S, Koellensperger G. Complementing reversed-phase selectivity with porous graphitized carbon to increase the metabolome coverage in an on-line two-dimensional LC–MS setup for metabolomics. Analyst. 2015; 140:3465–3473. [PubMed: 25824707]

[30]. McLafferty, FW. Interpretation of mass spectra. University Science Books; Herndon VA, USA: 1993.

[31]. Li S, Wilson WK, Schroepfer GJ Jr. New methods for determining the enantiomeric purity of *erythro*-sphingosine. J. Lipid Res. 1999; 40:764–772. [PubMed: 10191301]

[32]. Michell RH. Inositol derivatives: evolution and functions. Nat. Rev. Mol. Cell Biol. 2008; 9:151–161. [PubMed: 18216771]

[33]. Reynolds TB. Strategies for acquiring the phospholipid metabolite inositol in pathogenic bacteria, fungi and protozoa: making it and taking it. Microbiology. 2009; 155:1386–1396. [PubMed: 19383710]

[34]. Morita YS, Fukuda T, Sena CB, Yamaryo-Botte Y, McConville MJ, Kinoshita T. Inositol lipid metabolism in mycobacteria: biosynthesis and regulatory mechanisms. Biochim. Biophys. Acta Gen.Subj. 2011; 1810:630–641.

[35]. Newton GL, Ta P, Bzymek KP, Fahey RC. Biochemistry of the initial steps of mycothiol biosynthesis. J. Biol. Chem. 2006; 281:33910–33920. [PubMed: 16940050]

[36]. Flatt PM, Mahmud T. Biosynthesis of aminocyclitol-aminoglycoside antibiotics and related compounds. Nat. Prod. Rep. 2007; 24:358–392. [PubMed: 17390001]

[37]. Empadinhas N, Mendes V, Simoes C, Santos MS, Mingote A, Lamosa P, Santos H, Da Costa MS. Organic solutes in *Rubrobacter xylanophilus*: the first example of di-*myo*-inositol-phosphate in a thermophile. Extremophiles. 2007; 11:667–673. [PubMed: 17510735]

[38]. Yoshida K-I, Aoyama D, Ishio I, Shibayama T, Fujita Y. Organization and transcription of the *myo*-inositol operon, *iol*, of *Bacillus subtilis*. J. Bacteriol. 1997; 179:4591–4598. [PubMed: 9226270]

[39]. Yebra MJ, Zúñiga M, Beaufils S, Pérez-Martínez G, Deutscher J, Monedero V. Identification of a gene cluster enabling *Lactobacillus casei* BL23 to utilize *myo*-inositol. Appl. Environ. Microbiol. 2007; 73:3850–3858. [PubMed: 17449687]

[40]. Beall CJ, Campbell AG, Dayeh DM, Griffen AL, Podar M, Leys EJ. Single cell genomics of uncultured, health-associated *Tannerella* BU063 (Oral Taxon 286) and comparison to the closely related pathogen *Tannerella forsythia*. PLoS One. 2014; 9:e89398. [PubMed: 24551246]

[41]. Friedrich V, Pabinger S, Chen T, Messner P, Dewhirst FE, Schäffer C. Draft genome sequence of *Tannerella forsythia* type strain ATCC 43037. Genome Announc. 2015; 3:e00660–00615. [PubMed: 26067981]

[42]. Guerin ME, Korduláková J, Alzari PM, Brennan PJ, Jackson M. Molecular basis of phosphatidyl-*myo*-inositol mannoside biosynthesis and regulation in mycobacteria. J. Biol. Chem. 2010; 285:33577–33583. [PubMed: 20801880]

[43]. Wyss C. Dependence of proliferation of *Bacteroides forsythus* on exogenous *N*-acetylmuramic acid. Infect. Immun. 1989; 57:1757–1759. [PubMed: 2722237]

[44]. Jorge CD, Borges N, Santos H. A novel pathway for the synthesis of inositol phospholipids uses cytidine diphosphate (CDP)-inositol as donor of the polar head group. Environ. Microbiol. 2015; 17:2492–2504. [PubMed: 25472423]

Europe PMC Funders Author Manuscripts

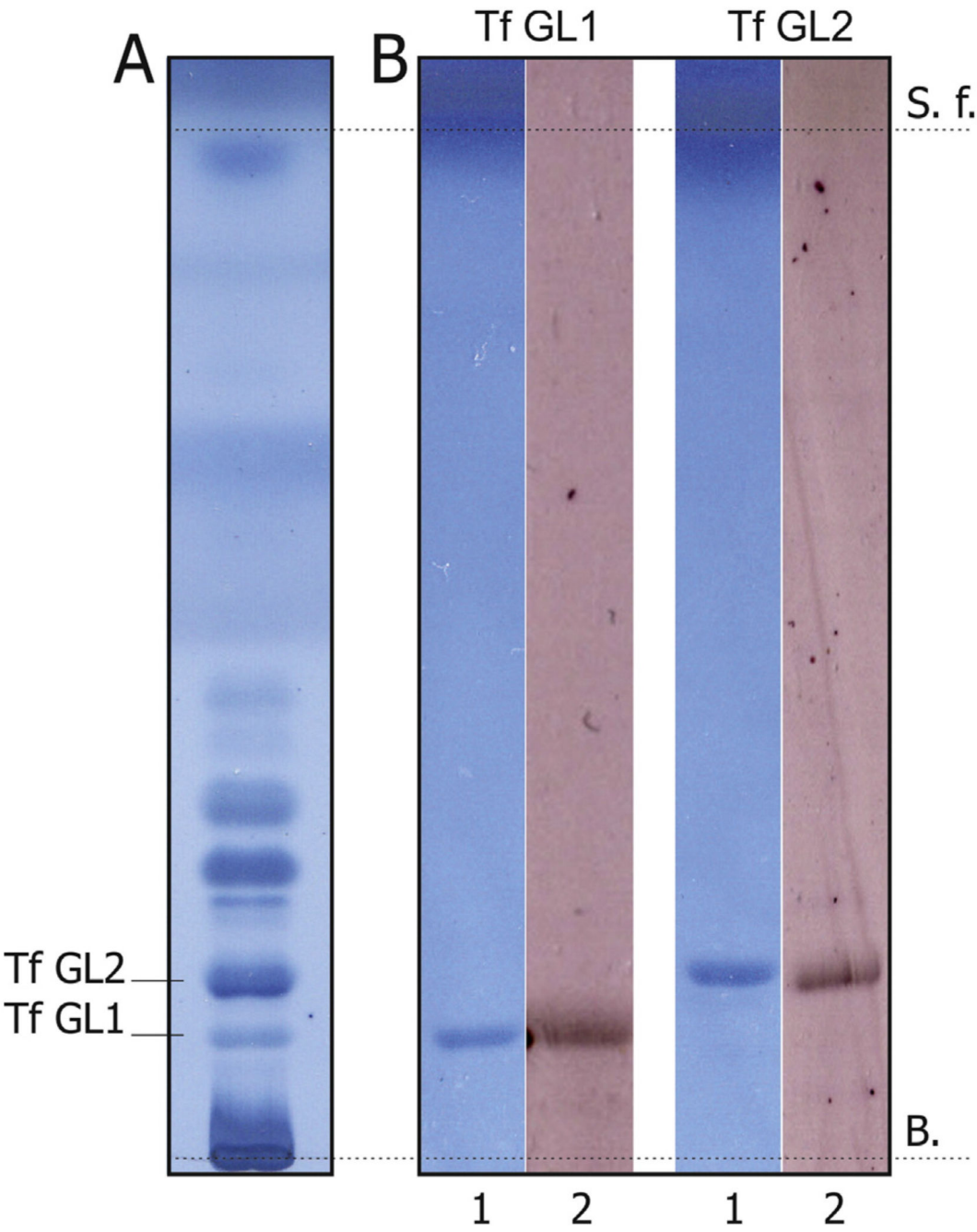

Fig. 1.

HPTLC of *T. forsythia* lipids developed with the solvent system chloroform: methanol:water (65:25:4). Visualization was performed with the Hanessian's stain for lipids (blue) and with thymol for carbohydrates (pink). Abbreviations: B., baseline; S. f., solvent front. A. Total lipid extract obtained using the Bligh–Dyer extraction method. 30 μg of sample were spotted at the baseline. TF GL1 and Tf GL2 ran at R_f values of 0.10 and 0.15, respectively. B. Purified Tf GL1 and Tf GL2 appeared as single bands in HPTLC and stained positive for carbohydrates. Lane 1: 3 μg of sample, lane 2: 10 μg of sample.

Europe PMC Funders Author Manuscripts

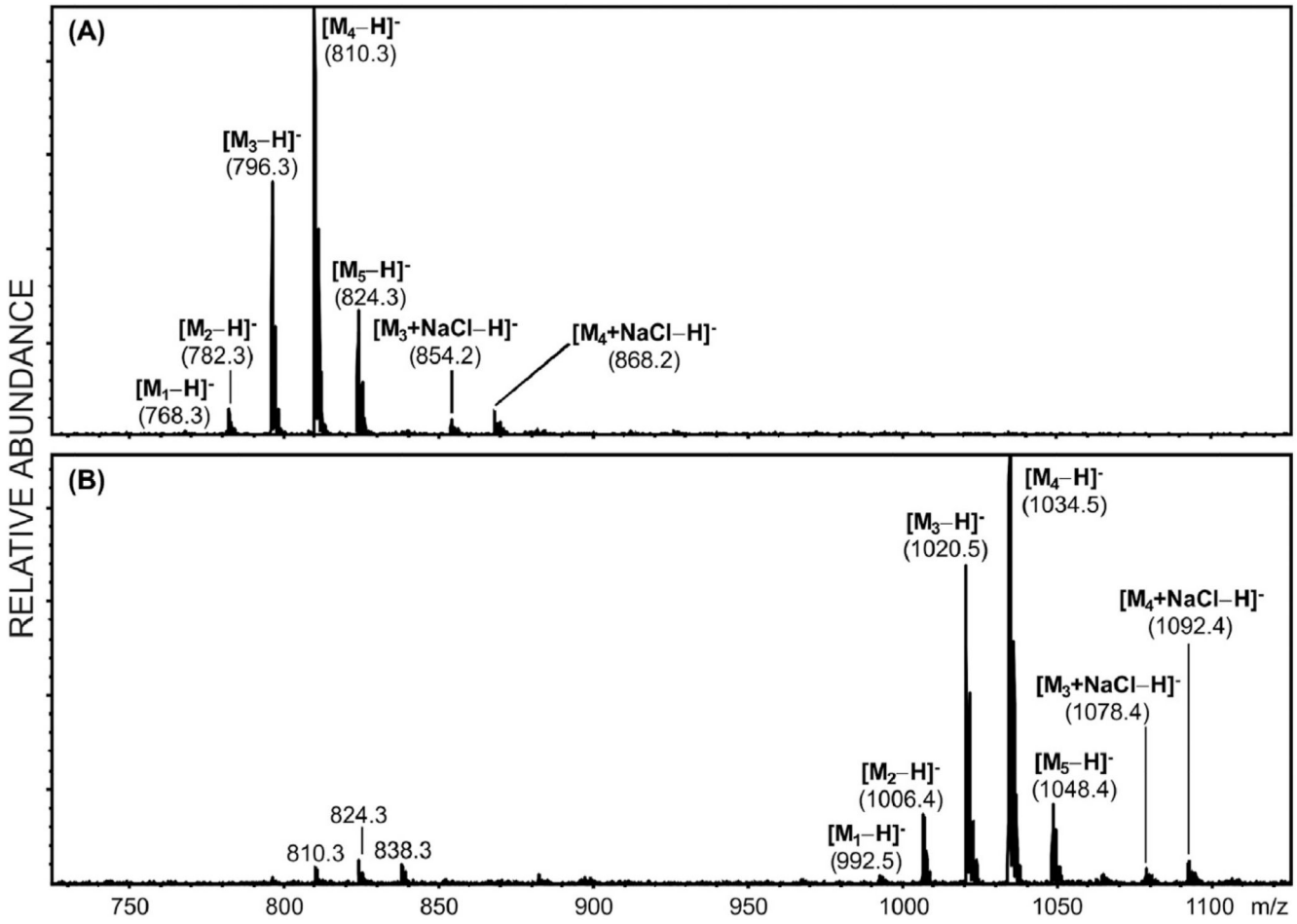

Fig. 2.

High-mass region of the negative-ion ESI-mass spectra ([M–H]$^{-}$, where M stands for the neutral mass of a given molecular species) of Tf GL1 (A) and Tf GL2 (B).

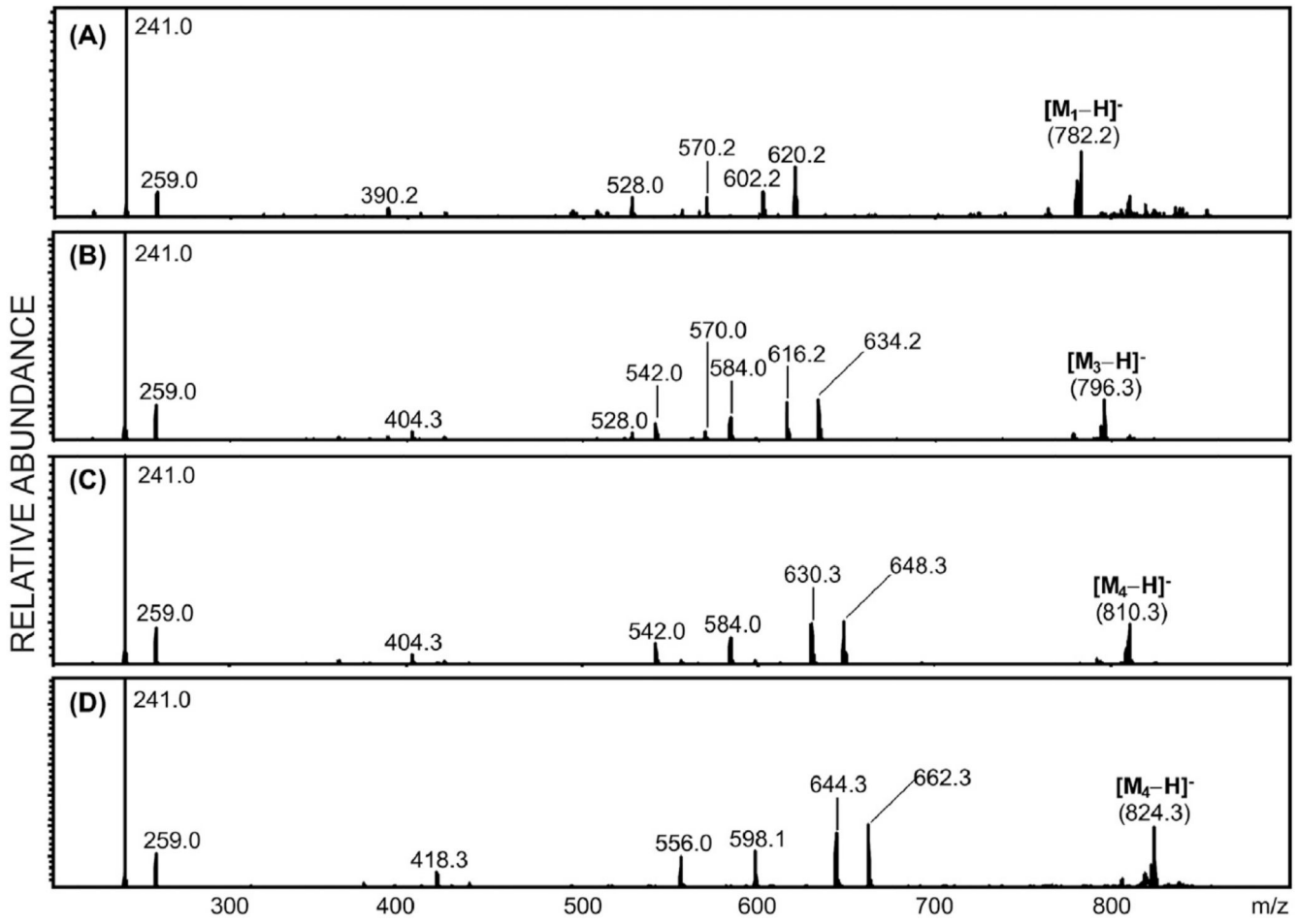

Fig. 3.

Negative-ion ESI low-energy CID–MS^2 of the Tf GL1 $[M–H]^-$ precursor ions: *m/z* 782 (A), *m/z* 796 (B), *m/z* 810 (C) and *m/z* 824 (D).

Europe PMC Funders Author Manuscripts

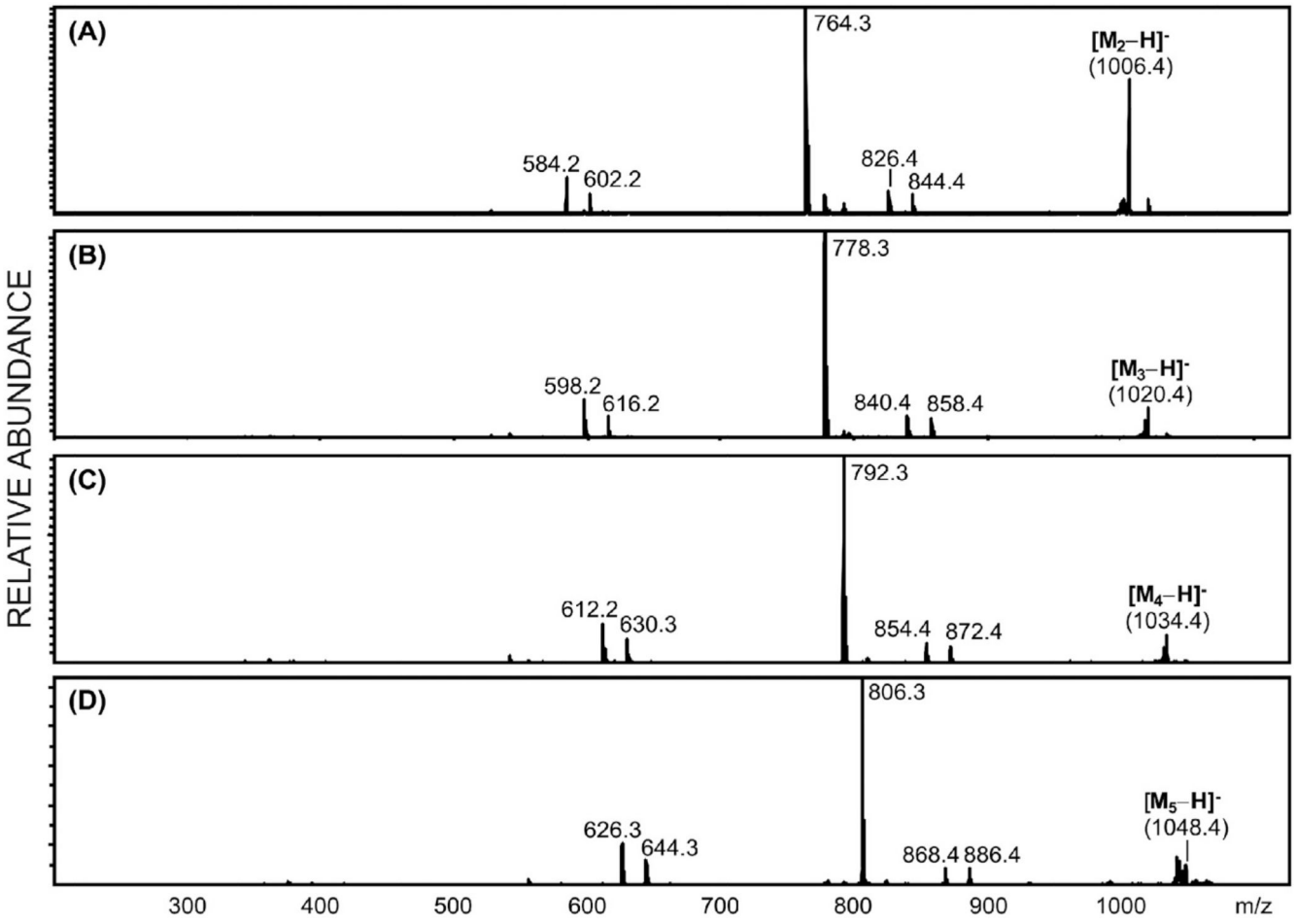

Fig. 4.

Negative-ion ESI low-energy CID-MS^2 of the Tf GL2 $[M–H]^-$ precursor ions: *m/z* 1006 (A), *m/z* 1020 (B), *m/z* 1034 (C) and *m/z* 1048 (D).

Europe PMC Funders Author Manuscripts

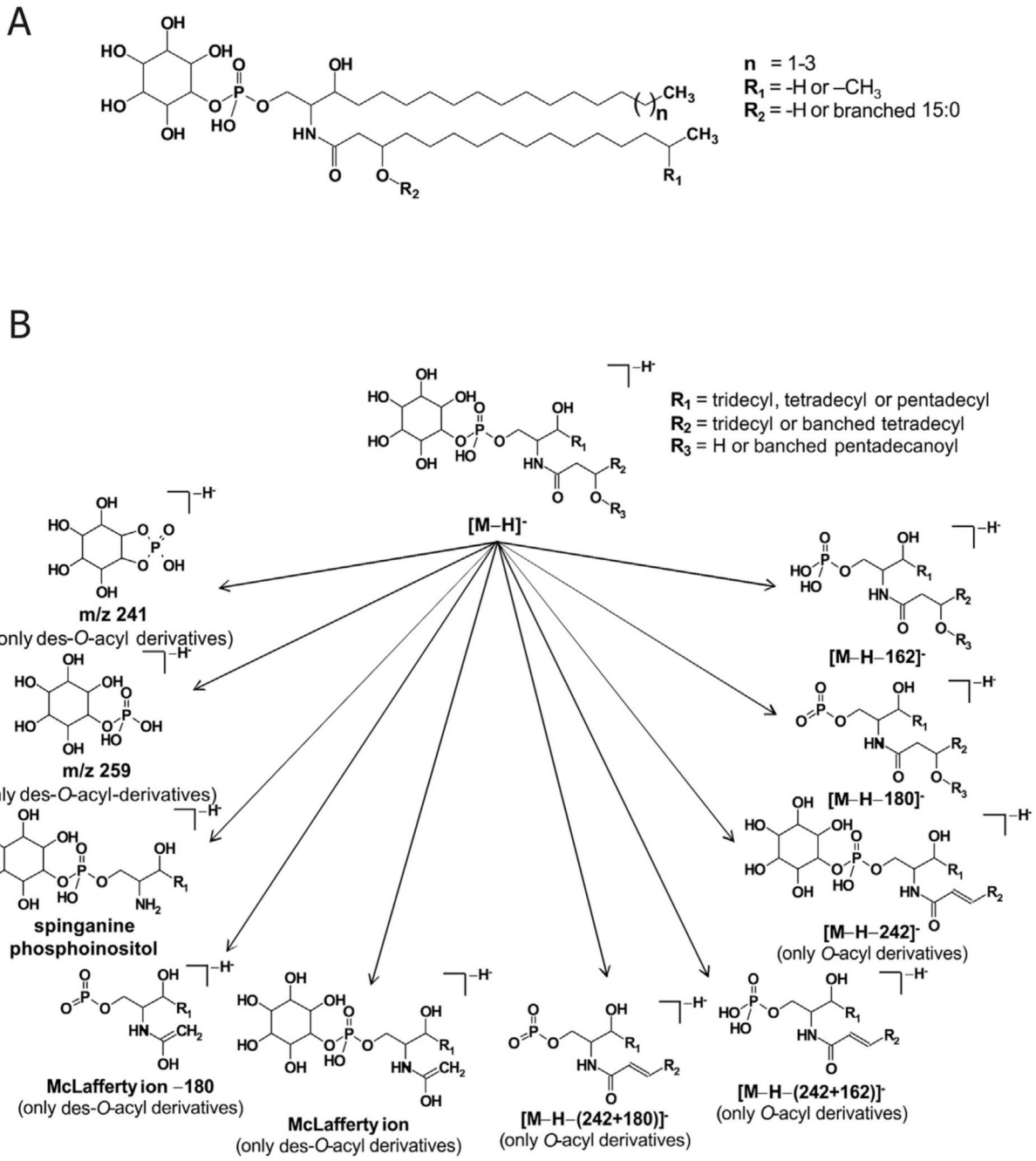

Fig. 5.

Structure (A) and general fragmentation pathways of [M–H]⁻ precursor ions of *O*-acyl-sphingo-phosphoinositols (Tf GL2) and *O*-deacyl-sphingo-phosphoinositols (Tf GL1) (B).

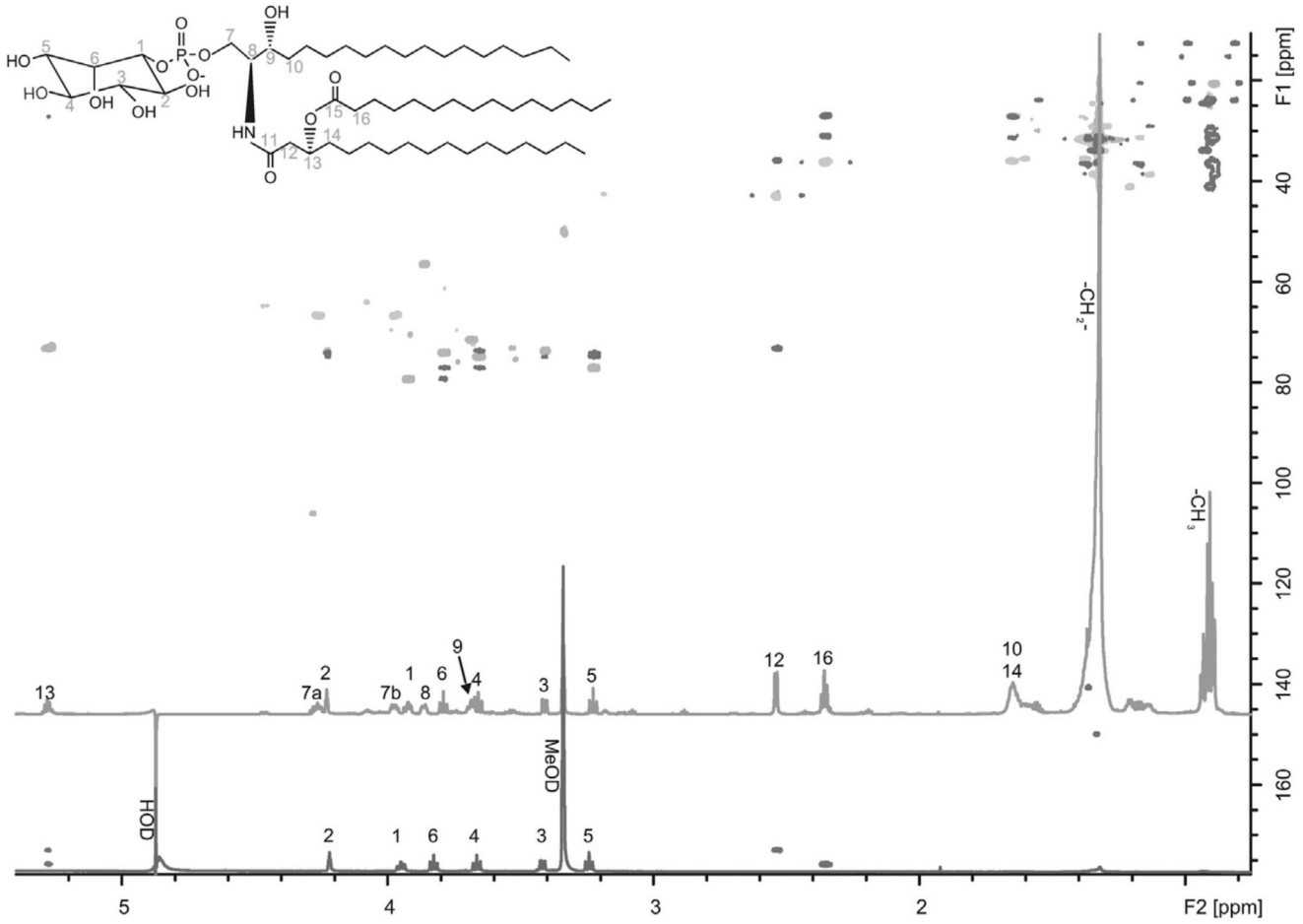

Fig. 6.

Overlay of the ^{1}H NMR spectra of 1-P-*myo*-inositol (black) and Tf GL2 (grey), along with the overlay of the 2D experiments HSQC-DEPT (grey dots) and HMBC (black dots). Numbers indicate the position in the structure of Tf GL2 (top, left). *Erythro*-sphinganine is drawn here in its D (8S, 9R) absolute configuration, however D- or L-configuration could not be distinguished.

Europe PMC Funders Author Manuscripts

Europe PMC Funders Author Manuscripts

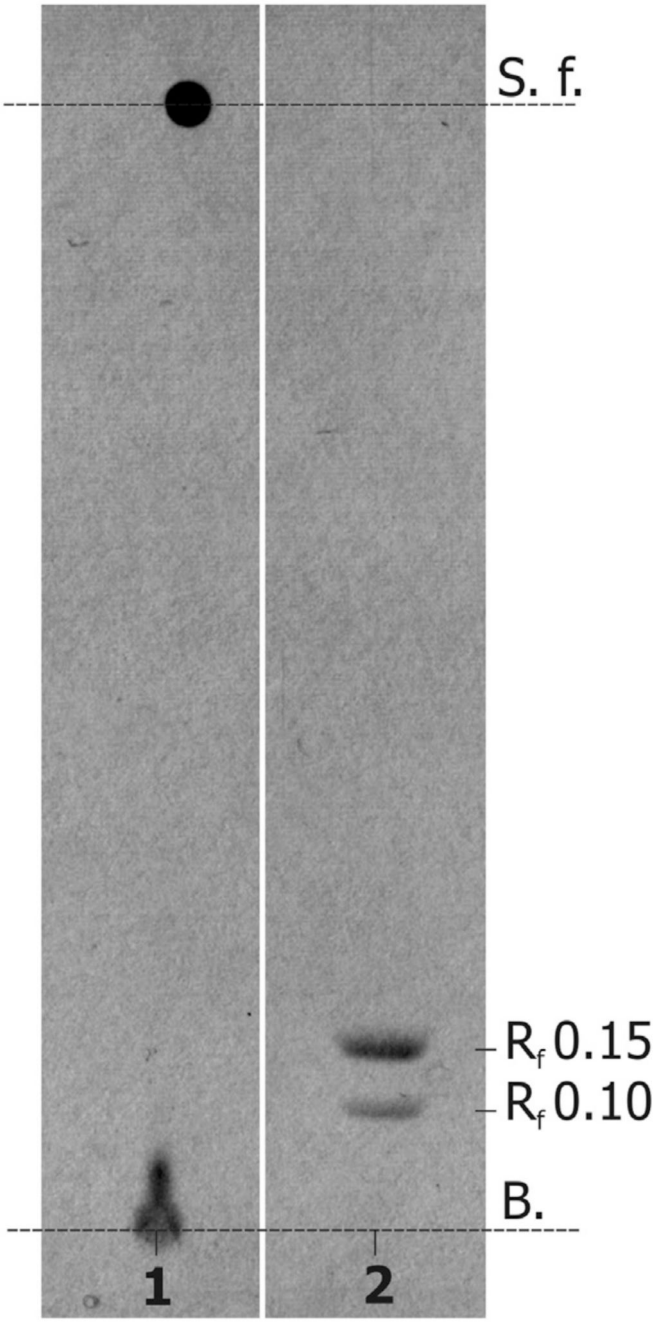

Fig. 7.

Autoradiography after HPTLC analysis of a total lipid extract of *T. forsythia* grown in the presence of [^{14}C(U)] *myo*-inositol. Lane 1 shows free [^{14}C(U)] *myo*-inositol which does not migrate in the solvent system used. Lane 2 shows the total lipid extract containing two lipid bands with incorporated [^{14}C(U)] *myo*-inositol with R_f values of 0.10 and 0.15 corresponding to Tf GL1 and Tf GL2, respectively. Abbreviations: B., baseline; S. f., solvent front; R_f, retardation factor.

Europe PMC Funders Author Manuscripts

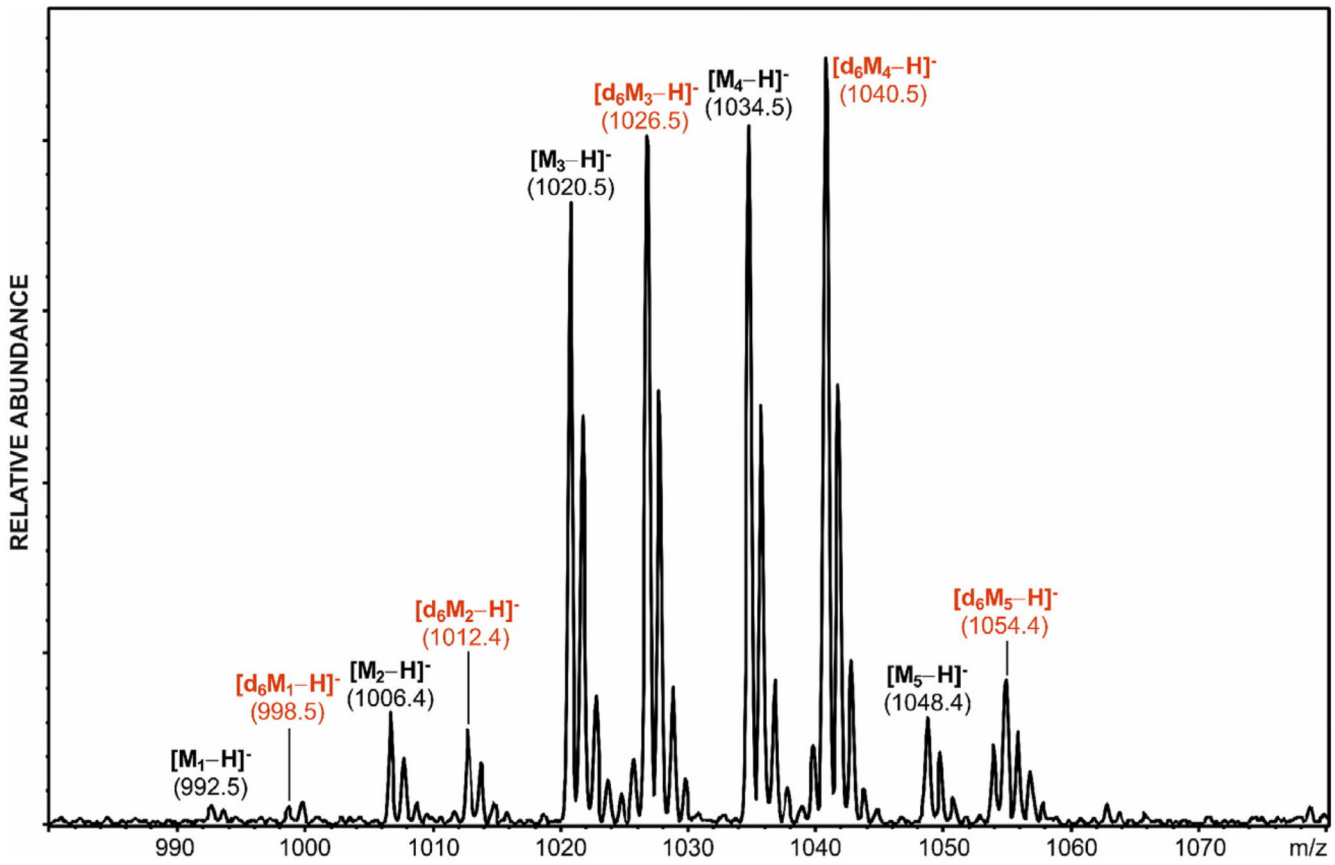

Fig. 8.

High-mass region of the negative-ion ESI-mass spectra of Tf GL2 isolated from *T. forsythia* grown in medium containing deuterium labeled and unlabeled inositol at a ratio of close to 1:1. Peaks labeled with $[d_6M–H]^-$ correspond to ions derived from deuterated inositol labeled Tf GL2, as indicated from the mass difference of 6 Da from the corresponding Tf GL2 $[M–H]^-$ ions.

Table 1

Combined GC–MS and ESI–MS data. Major losses and product ions of the $[M–H]^-$ precursor ions of the sphingo-phosphoinositols of Tf GL1 (A) and the corresponding *O*-acyl-sphingo-phosphoinositols of Tf GL2 (B). An asterisk (*) indicates those sphingolipid species containing additionally two diagnostic low-mass product ions for phosphoinositol at *m/z* 259 and at *m/z* 241 which are not detected for the *O*-acyl-sphingo-phosphoinositols (Tf GL2) due to the low mass cut-off of the 3D-ion trap instrument utilized for the experiments. Abbreviations: FA, fatty acid; Sph, sphinganine.

Sphingolipid species	**$[M–H]^-$**	**−162/−180 (loss of inositol)**	**−242 (loss of the *O*-linked 15:0 FA)**	**−(242 + 162/+180) (loss of inositol plus the *O*-linked 15:0 FA)**	**Partial loss of the *N*-linked OH–FA (McLafferty rearrangement) including additional loss of inositol**	**Loss of the *N*-linked OH–FA**
A						
*C_{33};Sph: 17:0; (N)HO–FA: 16:0 linear	782	620/602	–	–	570 (−180:390)	528
*C_{34};Sph: 17:0; (N)HO–FA: 17:0 branched	796	634/616	–	–	570 (−180:390)	528
*C_{34};Sph: 18:0; (N)HO–FA: 16:0 linear	796	634/616	–	–	584 (−180:404)	542
*C_{35};Sph: 18:0; (N)HO–FA: 17:0 branched	810	648/630	–	–	584 (−180:404)	542
*C_{36};Sph: 19:0; (N)HO–FA: 17:0 branched	824	662/644	–	–	598 (−180:418)	556
B						
C_{33};Sph: 17:0; (N)HO–FA: 16:0 linear, (O)FA: 15:0 branched	1006	844/826	764	602/584	–	528
C_{34};Sph: 17:0; (N)HO–FA: 17:0 branched, (O)FA: 15:0 branched	1020	858/840	778	616/598	–	528
C_{35};Sph: 18:0; (N)HO–FA: 17:0 branched, (O)FA: 15:0 branched	1034	872/854	792	630/612	–	542
C_{36};Sph: 19:0; (N)HO–FA: 17:0 branched, (O)FA: 15:0 branched	1048	886/868	806	644/626	–	556

Table 2

^{1}H, ^{13}C and ^{31}P NMR assignments of 1-P-*myo*-inositol and Tf GL2 and scalar correlations seen in the HMBC spectrum. Numbers in bold indicate the position in the structure of Tf GL2 as shown in Fig. 6. Multiplicity abbreviations: a, b, hydrogen atoms; d, doublet; t, triplet; m, multiplet; dd, double doublet.

	^{1}H (ppm)	^{13}C (ppm)	^{31}P (ppm)	HMBC (ppm)
1-*P*-*myo*-Inositol				
1	m 3.95	78.21	2.22	
2	t 4.22	73.95	–	
3	m 3.42	73.68	–	
4	t 3.66	74.72	–	
5	t 3.23	77.11	–	
6	t 3.82	74.28	–	
Tf GL2				
1	m 3.92	79.33	1.84	
2	t 4.23	73.93	–	
3	dd 3.41	73.68	–	
4	t 3.65	74.83	–	
5	t 3.22	77.03	–	
6	t 3.78	74.05	–	
7a	m 4.26	66.69	1.84	
7b	m 3.97			
8	m 3.86	56.43	–	**8** 3.86/**11** 172.98
9	m 3.68	71.45	–	
10a, b	1.68–1.61	27.02	–	
11	–	172.98	–	172.98
12	d 2.54	42.94	–	**12** 2.54/**13** 73.19
				12 2.54/**11** 172.98
13	m 5.27	73.19	–	**13** 5.27/**11** 172.98
				13.5.27/**15** 175.78
14a, b	1.68–1.64	27.02	–	**14** 1.66/**15** 175.78 (faint signal)
15	–	175.78	–	175.78
16a, b	t 2.35	36.12	–	**16** 2.35/**15** 175.78 (strong signal)